Title

Assessment of streamflow components and hydrologic transit times using stable isotopes of oxygen and hydrogen in waters of a subtropical watershed in eastern China

Authors

Hu, Minpeng
Zhang, Yufu
Wu, Kaibin
et al.

Publication Date

2020-10-01

DOI

10.1016/j.jhydrol.2020.125363

Peer reviewed

Journal of Hydrology 589 (2020) 125363

Contents lists available at ScienceDirect

Journal of Hydrology

journal homepage: www.elsevier.com/locate/jhydrol

Research papers

Assessment of streamflow components and hydrologic transit times using stable isotopes of oxygen and hydrogen in waters of a subtropical watershed in eastern China

Minpeng Hu[a,b], Yufu Zhang[a], Kaibin Wu[a], Hong Shen[a], Mengya Yao[a], Randy A. Dahlgren[d], Dingjiang Chen[a,c,*]

[a] College of Environmental & Resource Sciences, Zhejiang University, Hangzhou 310058, China
[b] Zhejiang Provincial Key Laboratory of Subtropical Soil and Plant Nutrition, Zhejiang University, Hangzhou 310058, China
[c] Ministry of Education Key Laboratory of Environment Remediation and Ecological Health, Zhejiang University, Hangzhou 310058, China
[d] Department of Land, Air, and Water Resources, University of California, Davis, CA 95616, USA

ARTICLE INFO

This manuscript was handled by Marco Borga, Editor-in-Chief, with the assistance of Daniele Penna, Associate Editor

Keywords:
Young water fraction
Mean transit time
Lag time
Watershed hydrology
Water resource management

ABSTRACT

Streamflow components (e.g., young water vs old water) and hydrological transit times play an important role in water resource and water quality management. We collected a four-year record of stable isotopes of oxygen and hydrogen ($\delta^{18}O$ and $\delta^{2}H$) in precipitation, groundwater and stream water for six catchments in the Yongan watershed of eastern China. The stable isotope records were used to identify spatio-temporal variations in the young water fraction (F_{yw}, defined as the proportion of the transit-time distribution younger than a threshold age) and mean transit time (MTT) based on sine-wave fitting and convolution integral methods, respectively. The F_{yw} ranged from 14 to 35% in the Yongan watershed. Cumulative transit time showed contrasting distributions, suggesting considerable heterogeneity and a complex interplay between catchment characteristics. Estimated MTTs ranged from 3.2 to 6.3 years and may be explained by catchment characteristics (e.g., elevation and topographic gradient). Observed spatial trends in MTTs likely result from contrasting contributions of different-aged subsurface water flows across the six catchments. The use of F_{yw} constraints in estimating MTTs reduced uncertainty in some catchments, suggesting the potential benefits of combining multiple approaches (e.g., F_{yw}) to optimize the results of traditional calibration methods. The relatively low F_{yw} and long MTTs highlight the importance of groundwater contributions to streamflow generation and imply a considerable lag time in river water quantity and quality responses to catchment-scale water resource management. Coupling multiple metrics (e.g., F_{yw} and MTT) and isotope models enhances our understanding of watershed-scale hydrologic processes and hydrograph separation.

1. Introduction

Efficient water resource management is critical for attaining regional and global sustainable development (Biswas, 2004). It is important to understand hydrological functions and water sources at the watershed scale to improve water management efficiency, especially given the potential impacts associated with future climate change. Fractions of young versus old water and transit time distributions are fundamental metrics used to describe the hydrological function of a catchment, which provides essential information for guiding management for water quality and quantity (Jasechko et al., 2016). Since streamflow generation is the product of climate, geology, soils, land cover and human activities, hydrological systems are highly variable over time and space (Davis Todd et al., 2007).

Stable isotopes of oxygen and hydrogen ($\delta^{18}O$ and $\delta^{2}H$) in waters are effective tracers for identifying stream water sources, hydrologic flowpaths and understanding hydrological processes across a range of spatial and temporal scales (McGuire and McDonnell, 2006; Klaus and McDonnell, 2013; Jasechko et al., 2016). Pinder and Jones (1969) first applied $\delta^{18}O$ and $\delta^{2}H$ in the 1970s to define event and pre-event water components based on a mass balance approach. In past decades, many studies have applied $\delta^{18}O$ and $\delta^{2}H$ for hydrograph separation in upland, forest and permafrost catchments across various geological and climatic regions (Klaus and McDonnell, 2013). Increasing evidences indicate that $\delta^{18}O$ and $\delta^{2}H$ coupled with watershed hydro-climate and hydrologic attributions provide an effective approach for exploring

* Corresponding author at: College of Environmental & Resource Sciences, Zhejiang University, Hangzhou 310058, Zhejiang Province, China.
E-mail address: chendj@zju.edu.cn (D. Chen).

https://doi.org/10.1016/j.jhydrol.2020.125363
Received 13 December 2019; Received in revised form 26 July 2020; Accepted 28 July 2020
Available online 02 August 2020
0022-1694/

hydrological components and processes (Hangen et al., 2001; McGuire and McDonnell, 2010). Relying on $\delta^{18}O$ and $\delta^{2}H$, previous studies explored the influence of soil types, land use/land cover, and rainfall characteristics (e.g., storm size and intensity) on streamflow components (Buttle, 1994; Kværner and Kløve 2006; Klaus and McDonnell, 2013).

Since records for $\delta^{18}O$ and $\delta^{2}H$ are often sparse and irregular in many studies, the sine-wave fitting method based on seasonal changes in the composition of stable isotopes in precipitation at temperate latitudes was developed to estimate the young water fraction (F_{yw}) of streamflow (Kirchner, 2016). The young water fraction likely represents shallow water flows (e.g., overland flow and fast subsurface lateral flow through upper soil horizons), while the remaining fraction is mainly derived from relatively deeper water flows in systems without large lakes/reservoirs. Therefore, F_{yw} provides an alternative and advantageous metric for quantifying watershed hydrological processes and components (young and old water fractions).

Since 2016, the isotope based sine-wave fitting method has been increasingly applied to estimate F_{yw}, as well as relevant solute dynamics (e.g, Na^{+}, silicon), in watersheds with different catchment sizes and characteristics (Clow et al., 2018). Previous studies determined that F_{yw} varies between < 5% to > 90% in different locations and time periods according to landscape and climate (Table S1). For example, some studies reported that topographic characteristics were the main factor influencing F_{yw}, including topographic gradient, elevation and drainage density (Jasechko et al., 2016, 2017; Clow et al., 2018). Other studies suggested precipitation, rainfall intensity and groundwater levels were important factors (von Freyberg et al., 2017; Wilusz et al., 2017; Wang et al., 2018). In contrast, a study across 22 contrasting catchments in Germany found no significant correlations between F_{yw} and catchment characteristics (Lutz et al., 2018). As a relatively new metric in hydrological studies, additional application to a wide range of hydrologic conditions is required to test the F_{yw} metric and determine the main factors influencing F_{yw} at the watershed scale. Furthermore, in spite of the reliability of F_{yw} in determining transit times in heterogeneous and nonstationary catchments, few studies have utilized this new metric to constrain model calibration when determining transit time distribution (TTD) and mean transit time (MTT) (Lutz et al., 2018).

Water transit time is a fundamental descriptor providing information on hydrological processes, water sources, flow paths and water storage within a given watershed (McGuire and McDonnell, 2006). Transit times are commonly inferred by identifying the variations of natural tracer signals in hydrologic inputs (precipitation) and outputs (stream water) using time-based convolution and sine-wave fitting methods (McGuire and McDonnell, 2006; Kirchner, 2016). However, the sine-wave fitting method can lead to large aggregation biases in MTT estimates for spatially heterogeneous, real-world catchments, which arise from the strong nonlinearity in the relationship between tracer cycle amplitude (A_S/A_P) and MTT (Kirchner, 2016). Besides the sine-wave fitting method, the convolution integral method defines the initial shape of the TTD for a given catchment, and further simulates the best-fit output tracer signal by combining the previous tracer inputs and calibrated TTDs (McGuire and McDonnell, 2006). The predefined TTD (e.g., exponential versus gamma distribution or two-parallel linear reservoirs) can introduce uncertainty in MTT estimates of real-world catchments, especially as impacted by parameter equifinality (Seeger and Weiler, 2014; Lutz et al., 2018). Therefore, the calibrated TTD parameters need be appropriately constrained. Although previous studies have presented some estimates for TTD and MTT parameter ranges and uncertainties (Hrachowitz et al., 2010; Timbe et al., 2014), few studies have utilized F_{yw} to improve estimates of TTD and MTT, or combined F_{yw} and MTT results to advance the understanding of watershed-scale hydrological processes (Lutz et al., 2018).

Previous studies utilizing stable isotopes of oxygen and hydrogen in waters in China mainly explored variations in the isotopic composition of precipitation across China, with limited data available for rivers (Li et al., 2015), especially in subtropical regions. The subtropical regions of China have a large number of rivers and lakes, which experience distinct seasonal variations due to much higher sunlight intensity, temperature and precipitation in summer than in winter. High evapotranspiration and intensive human activities, coupled with the complexity of hydrological functions, cause serious challenges to regional water resource management (Mokhtar et al., 2020). Therefore, it is strongly warranted to investigate variations in the isotopic composition of water isotopes to better constrain hydrologic metrics, such as F_{yw} and MTT, to improve our understanding of hydrological function and water sources in subtropical river systems.

Based on four years of monthly $\delta^{2}H$ and $\delta^{18}O$ measurements in precipitation, groundwater and streamflow water across six catchments in the Yongan watershed of eastern China, this study (1) interpreted catchment-scale stable isotope signals; (2) estimated F_{yw} (Kirchner, 2016) and combined it with the two-parallel linear reservoirs (TPLR) model to determine MTTs for the catchments; and (3) assessed the potential role of hydro-climatic characteristics on regulating the spatio-temporal variations in F_{yw} and MTTs. As the first integrated application to subtropical watersheds, results of this study fill a "gap" in $\delta^{18}O$ and $\delta^{2}H$ maps for subtropical regions, and further provide insights for identifying hydrological processes and understanding nutrient transport lag times for a large geographical area.

2. Material and methods

2.1. Study area

The Yongan watershed (120.23–121.01°E and 28.47–29.04°N; elevation ~15–1000 m) is a typical rainfall-dominated, forest and agricultural watershed in the subtropical region of southeastern China. The Yongan River is the third largest river of Zhejiang province and flows to the East China Sea, draining 2,474 km^2 and having an average discharge of 72.9 $m^3\ s^{-1}$ at the downstream BZA sampling site (Fig. 1). The river has no large dams or transboundary water withdrawals. Climate is subtropical monsoon with an average annual temperature of 17.4 °C. Average annual precipitation and evapotranspiration were 1528 mm and 1016 mm, respectively, during the four year study period (2014–2018, Fig. 2 and Fig. S3). Rainfall mainly occurs in May–October, with a typhoon season in July–September (Fig. S1). The water year was separated into four hydrologically contrasting seasons: spring (March-May), summer (June-August), autumn (September-November) and winter (December-February). Daily temperature and evapotranspiration showed strong seasonal variation, with higher values observed in spring and summer (Fig. 2b). The number of rainy days decreased by more than 20 days while storm event frequency (> 50 mm per 24 h) increased by 65–76% in the past 30 years (Chen et al., 2014b), which intensified seasonal drought (November to April) and flooding issues (May to September). The majority of agricultural irrigation/drainage systems used in 1980–1999 were constructed with stone and mud in the 1950s and continuously lost water delivery capacity due to silting and collapse. Therefore, agricultural lands have become waterlogged during the rainy season (May–September), especially during the typhoon season (Fig. S1), resulting in considerable crop yield reduction.

Agricultural land, including paddy field, garden plots (vegetable farm and orchard) and rain-fed crops averaged ~12% of total watershed area in recent decades, with developed lands, forest and barren land (including surface waters, wetlands, rock and wildlands) contributing ~3, ~67 and ~18%, respectively. The mountainous region is mostly composed of volcanic and clastic rocks. Red (Oxisols), yellow (Ultisols) and lithological (Entisols) soil groups accounted for 64.6%, 15.4% and 1.5% of total soil area, respectively (Chen et al., 2014b). Alluvial and paddy soil groups were the dominant soil types in the low elevation region and accounted for 3.9% and 14.6% of total soil area, respectively. Among the six catchments examined in this study, SJY and

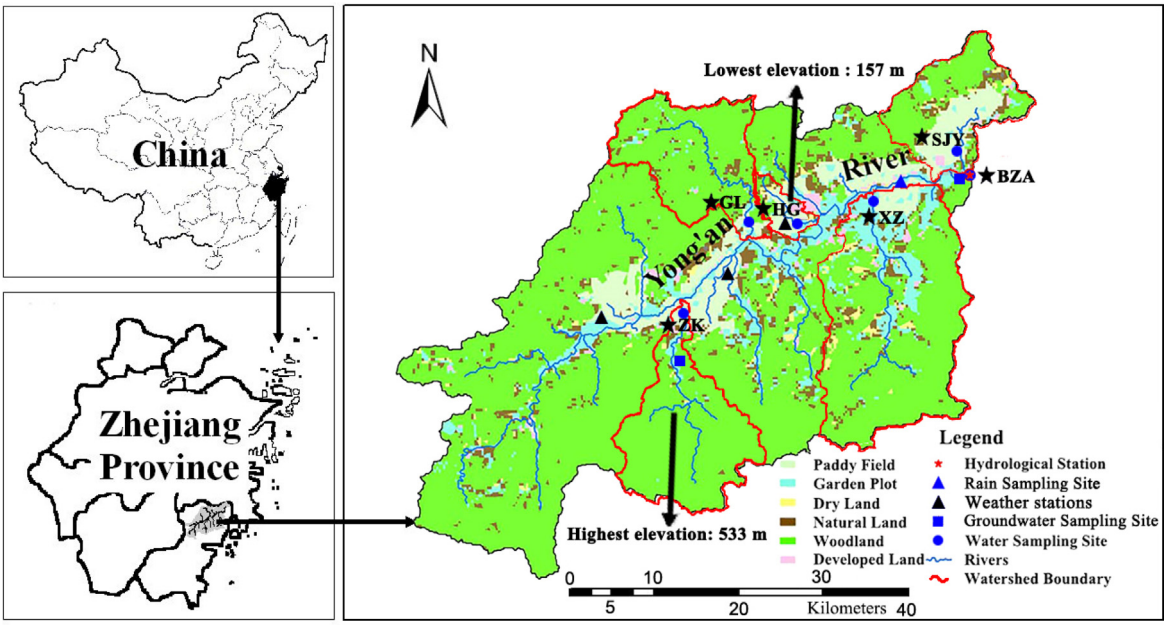

Fig. 1. Land-use in Yongan watershed, Zhejiang Province, China with meteorological, precipitation and stream water sampling locations. The mean elevation in catchment HG is lowest, while that in catchment ZK is highest.

ZK had the highest (20%) and lowest (2%) percentages of paddy fields, as well as agricultural lands (Table 1).

Since river water flow data for individual sub-catchments were not available, we estimated the discharge from the daily discharge measurements at the downstream monitoring site (BZA) using the fractional area of each sub-catchment relative to the entire watershed. This approach was consistent with measured discharge available for the SJY sub-catchment (R^2 = 0.79, Fig. S5). Land-use distribution and catchment characteristics (e.g., mean elevation, topographic gradient, channel length, catchment area and topographic wetness index) (Beven and Kirkby, 1979; Sörensen et al., 2006) were derived from a 2009 DEM (30-m resolution) of the watershed using ArcGIS 10.3. Drainage densities (DDs) were computed as the ratio of channel length to catchment area.

2.2. Field sampling and laboratory methods

River water samples were collected at the six catchment outlets once

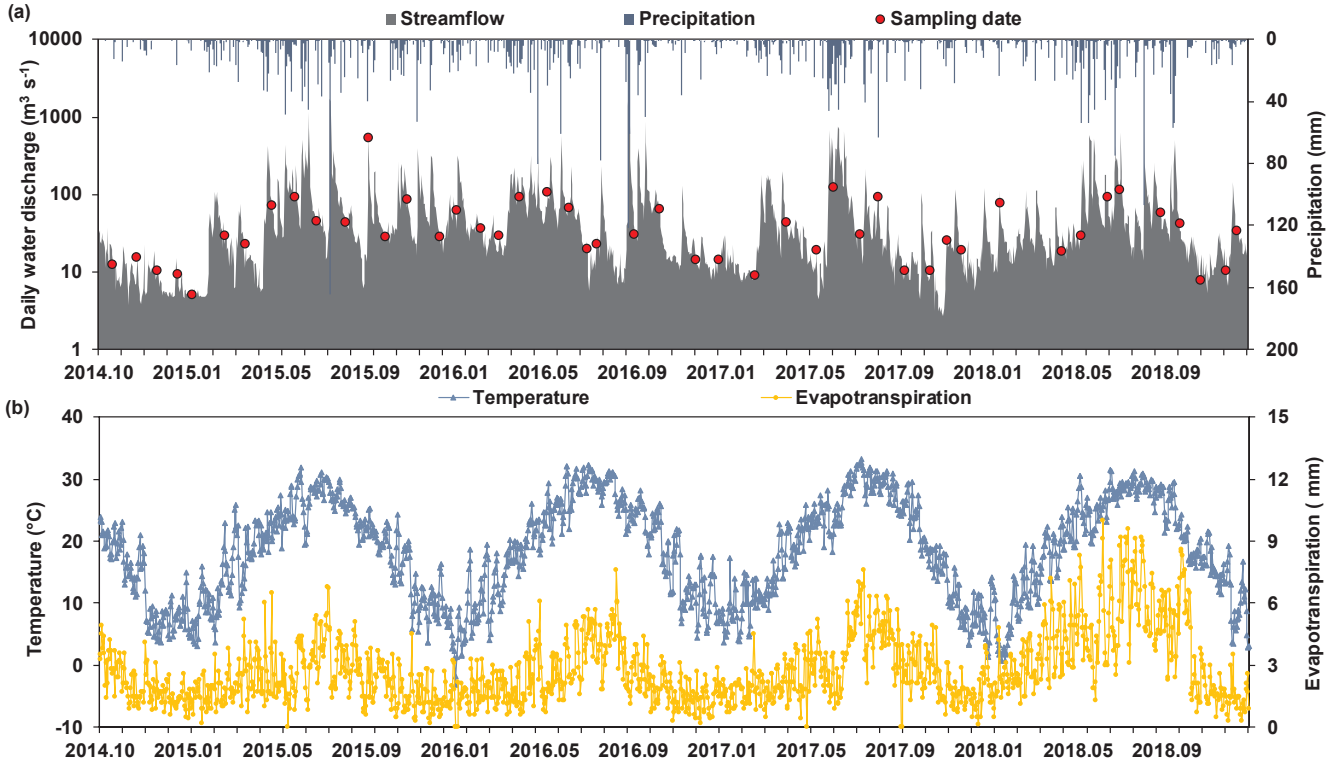

Fig. 2. (a) Daily precipitation, discharge and (b) evapotranspiration and temperature in the Yongan watershed in 2014–2018.

Table 1
Catchment characteristics and land-use distribution for the six catchments in the Yongan watershed.

Catchments	Area (km^2)	A (%)	D (%)	F (%)	N (%)	PF (%)	Mean Elevation (m)	Topographic gradient (%)	TWI	Drainage density (km km^{-2})
XZ	357	11	2	74	13	6	359	19.0	6.21	2.22
HG	35	21	9	49	21	10	157	7.5	7.68	1.86
SJY	163	44	1	54	1	20	291	14.8	6.84	2.33
ZK	218	3	1	76	20	2	533	24.6	5.82	2.24
GL	202	14	1	70	14	6	351	20.2	6.02	2.03
Entire watershed (BZA)	2474	13	3	67	17	6	438	18.2	6.35	2.28

A - agricultural lands, D - developed lands, F - forest lands, N - non-utilized lands, PF - paddy field. TWI (unitless) - topographic wetness index.

every 4 weeks during the 2014–2018 study period for a total of 38–47 samples at each site (Fig. 1). Correspondingly, groundwater samples were collected at wells located in the BZA (~18 m vertical depth from land surface, n = 47) and ZK (~4 m vertical depth from land surface, n = 42) catchments once every 4 weeks during the study period (Fig. 1). Rainfall samples were collected near the weather station (Station C, Fig. S4) on an event basis and composited into monthly samples with volume-weighting. All water samples were immediately sealed and stored at 4 °C to prevent fractionation due to evaporation. Isotopic analysis of water samples was performed using an isotope-ratio mass spectrometer (Delta V Advantage, Thermo Scientific). Stable isotope composition for oxygen and hydrogen in water is reported in δ notation (‰, parts per thousand) based on Vienna Standard Mean Ocean Water (VSMOW) (e.g., $\delta^{18}O = [(^{18}O/^{16}O_{sample})/(^{18}O/^{16}O_{VSMOW}) - 1] \times 1000‰$) (Brand et al., 2014). Two internal standards calibrated against VSMOW (Biscayne Aquifer Drinking Water (USGS45) and Lake Louise Drinking Water (USGS47) were used to calibrate raw data and ensure long-term stability of analyses. The analytical precision was ± 0.2‰ for $\delta^{18}O$ and ± 1‰ for $\delta^{2}H$. Volume-weighted mean values (M_v) for each season were calculated as follows:

$$M_v = \frac{\sum_i \delta^{18}O_i * Q_i}{\sum_i Q_i} \quad (1)$$

where $\delta^{18}O_i$ and Q_i are the isotope value and precipitation volume for a given season, respectively. Daily river discharge for downstream site BZA was obtained from the local Hydrology Bureau. Daily evapotranspiration and daily precipitation (2005–2018) for the watershed were obtained from the local Weather Bureau. Evapotranspiration measures followed national specifications for surface meteorological observation (GB/T 35230-2017) using a pan evaporator (E601B model) in the weather station.

2.3. Young water fraction calculation

This study adopted the isotope-based sine-wave fitting method to estimate F_{yw}, which is based on the damping and phase-shifted isotopic signals between precipitation and river water (Kirchner, 2016). The sine-wave fitting method based on water isotopes was conducted for all six catchments using data for 2014.09–2018.12. Sine waves were fitted with the $\delta^{18}O$ (‰) time series (most commonly used in previous studies, McGuire and McDonnell, 2006):

$$C_p(t) = a_p \cos(2\pi ft) + b_p \sin(2\pi ft) + k_p$$
$$C_s(t) = a_s \cos(2\pi ft) + b_s \sin(2\pi ft) + k_s \quad (2)$$

$$A_p = \sqrt{a_p{}^2 + b_p{}^2},\ A_s = \sqrt{a_s{}^2 + b_s{}^2} \quad (3)$$

$$\varphi_P = \arctan(b_P/a_P),\ \varphi_S = \arctan(b_S/a_S) \quad (4)$$

In Eqs. (2)–(4), $C_p(t)$ and $C_s(t)$ are the tracer signal ($\delta^{18}O$) for precipitation and streamflow at time t, f is the frequency of the cycle (set to 1/365 days), k_P and k_S represent the vertical shift of the sine wave, and a_p, b_p, a_s and b_s are coefficients for determining the amplitude (i.e., A_P and A_S) and phase shift (i.e., φ_P and φ_S) of seasonal cycles. F_{yw} was calculated as the amplitude ratio A_S/A_P, which has proven effective for estimating the young water fraction (Kirchner, 2016).

2.4. Transit-time distribution (TTD) calculation

Stable isotopes are widely usedfor estimating TTDs and MTTs (McGuire et al., 2005; Hale and McDonnell, 2016; Lutz et al., 2018). We used composited precipitation from 2014.09.30 to 2018.12.07 as isotope inputs to simulate stream water isotopes with the lumped-parameter convolution method. Similar to the methodology of Stockinger et al. (2016), we estimated effective precipitation (P_{eff}) using the non-linear Antecedent Precipitation Index (API) approach (Jakeman and Hornberger, 1993):

$$p_{eff} = p(t)s(t) \quad (5)$$

$$s(t) = b_1 p(t) + (1 - b_2^{-1})s(t - \Delta t) \quad (6)$$

where $p(t)$ is precipitation, $s(t)$ is API, Δt is the calculation time step of one day, b_1 is a scaling factor to match the amount of total simulated runoff to the amount of total p_{eff}, and b_2 is a weighting for each precipitation event backward in time. The initial API condition was set as 0.

The TTD was estimated by fitting the isotope tracer signal of stream water (Stockinger et al., 2016):

$$C_s(t) = \frac{\int_0^t C_p(t-\tau)p_{eff}((t-\tau))h(\tau)d\tau}{\int_0^t p_{eff}(t)h(\tau)d\tau} \quad (7)$$

where $C_s(t)$ is the simulated stream water isotope concentration at time t, $p_{eff}(t\text{-}\tau)$ is effective precipitation for time $t\text{-}\tau$, and $C_p(t\text{-}\tau)$ is precipitation isotope concentration at time $t\text{-}\tau$ with transit time τ and TTD $h(\tau)$, which is calibrated during the stream water isotope concentration simulation.

Hrachowitz et al. (2009) demonstrated the reliability of the two-parallel linear reservoirs (TPLR) approach to capture the short- and long-term fluctuations of stream discharge in response to input variations. Therefore, we adopted the TPLR approach to simulate TTDs. The TPLR approach divides TTDs into a fast and slow response reservoir, which allows for a more realistic characterization of flow path distributions (Weiler et al., 2003; Stockinger et al., 2016):

$$h(\tau_t) = h_f(\tau_t) + h_s(\tau_t) = \frac{\theta}{\tau_f}\exp\left(-\frac{\tau}{\tau_f}\right) + \frac{1-\theta}{\tau_s}\exp\left(-\frac{\tau}{\tau_s}\right) \quad (8)$$

where $h_f(\tau_t)$ and $h_s(\tau_t)$ are the flow path distributions for the fast and slow responding reservoirs, and θ is a factor (from 0 to 1) that partitions the input into the fast responding reservoir. According to the definition of the F_{yw} metric, it is conceptually consistent with the fast responding reservoir. The factor θ was thus assumed to be analogous to the young water fraction estimated by the sine-wave fitting method, thereby providing a constraint for simulating stream water isotopes in this study. According to previous studies (Wilusz et al., 2017; Lutz et al., 2018; Bansah and Ali, 2019), the young water age threshold was assumed as < 90 days (Table S1).

Parameters τ_f and τ_s in Eq. (8) are the mean transit times of the fast and slow reservoirs, respectively. Thus, MTT was calculated as:

$$MTT = \tau_f * \theta + \tau_s * (1 - \theta) \quad (9)$$

A model warm-up period from 2010 to 2017 was used to "prime" the model before fitting the measured $\delta^{18}O$ from stream water samples. Since the long-term water isotope values for precipitation before 2014 were not available, we set the warm-up data as the average value of the measured $\delta^{18}O$ values for precipitation during our study period. We calibrated Eq. (9) to optimize parameters using the Particle Swarm Optimization (PSO) algorithm (Kennedy and Eberhart, 1995, Lutz, et al., 2018) in R software (Ver. 3.6.1). Model efficiency was evaluated in terms of Nash-Sutcliffe Efficiency (NSE) to achieve the best stream water isotope concentration simulation results (Nash and Sutcliffe, 1970):

$$NSE = 1 - \frac{\sum (C_{obs} - C_{sim})^2}{\sum (C_{obs} - \bar{C_{obs}})^2} \quad (10)$$

where C_{obs} and C_{sim} are observed and simulated stream water isotope concentrations, respectively.

We conducted a sensitivity analysis to examine the importance of each parameter (i.e., θ, τ_f and τ_s) in determining MTT results. Uncertainty analysis was conducted for A_s and A_p using the Markov Chain Monte Carlo (MCMC) search procedure with the DREAM-ZS algorithm in MATLAB (Vrugt, 2016). We ran the search procedure for 20,000 iterations using 5 parallel chains to find the parameter set that maximized the log-likelihood function. Results from the remaining 5000 iterations were used in the uncertainty estimation (95%-confidence limits). After uncertainty estimations for A_s/A_p (i.e., F_{yw}) were determined, the 95%-confidence intervals were further adopted as the parameter distribution of θ to constrain MTT estimates. Ranges of F_{yw} values were used to calibrate best-fit parameters for the stable isotope signals of stream water with the PSO algorithm; 10,000 simulations for each catchment were calculated in R software (Ver. 3.6.1). The posterior 5,000 groups of parameters (i.e., θ, τ_f and τ_s) were used to determine the 95%-confidence limits for MTTs in each catchment. Spatial and temporal variations in δ^2H and $\delta^{18}O$ were examined using one-way ANOVA. Pearson's correlation and regression analyses were used to explore relationships between catchment characteristics and F_{yw}, MTTs, and $\delta^{18}O$ values. Statistical analyses were conducted in MATLAB (Ver. 10.0, MathWorks, Natick, MA, USA).

3. Results and discussion

3.1. Temporal and spatial variations in isotope signals

During the study period (2014.09–2018.12), $\delta^{18}O$ and δ^2H values in precipitation ($\delta^{18}O$: −14.6 to −0.6‰ and δ^2H: −103.5 to 20.7‰), groundwater ($\delta^{18}O$: −10.2 to −4.0‰ and δ^2H: −56.0 to −26.9‰) and stream water ($\delta^{18}O$: −11.5 to −4.3‰ and δ^2H: −60.2 to −26.9‰) presented high variability over time and space in the Yongan watershed (Table 2). Similar results were observed in $\delta^{18}O$ (−14.7 to −3.0‰) and δ^2H values (−102.4 to −32.2‰) for several major rivers in China (e.g., Yangtze River, Yellow River, Pearl River; Li et al., 2015), as well as in the $\delta^{18}O$ (−8.2 to −4.1‰) for rivers of nearby regions (Fig. 3a; Hu et al., 2013; Ji et al., 2017). Furthermore, the mean stable isotope values observed in stream water for the entire watershed (site BZA - δ^2H: −42.8‰ and $\delta^{18}O$: −6.9‰) were well within those observed in the five tributaries (δ^2H: −45.0‰ to −38.0‰ and $\delta^{18}O$: −7.5‰ to −6.2‰), which indirectly supports the reliability of our measured results. The high variability observed in $\delta^{18}O$ and δ^2H values across precipitation, groundwater and stream water results from interactions among dilution, enrichment and attenuation processes along the land–freshwater continuum (Kirchner, 2016), implying appreciable heterogeneity in water cycling processes at the watershed scale.

The slope of the Local Meteoric Water Line (LMWL) for precipitation in the Yongan watershed ($\delta^2H = 7.58\delta^{18}O + 14.66‰$, n = 43, $R^2 = 0.91$, $p < 0.001$) was similar to the Global Meteoric Water Line (GMWL: $\delta^2H = 8\delta^{18}O + 10‰$) (Fig. 4a; Craig, 1961). In contrast, regression line slopes for both stream water ($\delta^2H = 5.01\delta^{18}O - 7.75‰$, n = 264, $R^2 = 0.69$, $p < 0.001$) and groundwater ($\delta^2H = 3.64\delta^{18}O - 17.77‰$, n = 89, $R^2 = 0.59$, $p < 0.001$) were considerably lower than the GMWL and LMWL of precipitation (Fig. 4b, c). The line-conditioned excess (lc-excess; Landwehr and Coplen, 2006) was estimated to assess the fractionation effect of evapotranspiration. The lc-excess value was more extreme for samples that deviated from LMWL, likely because of evapotranspiration. The lc-excess values in different catchments ranged from −5.85 to −3.17‰ (mean: −4.36‰, Table 2), suggesting some differences in evapotranspiration among catchments. The different slopes between LMWL and regression lines for stream water and groundwater further indicate the importance of evapotranspiration (> 1000 mm yr^{-1}), consistent with the measured daily evapotranspiration for our catchments (Fig. 2). The lower slopes for stream water and groundwater result from watershed evapotranspiration, since $\delta^{18}O$ will become more enriched in stream water than δ^2H during evapotranspiration (Gonfiantini, 1986). This increases the oxygen and hydrogen isotopic values in the residual fraction and generates a systematic deviation from the LMWL (Sánchez-Murillo et al., 2015). Water bodies in subtropical regions experience relatively high evapotranspiration (Babkin, 2009), which contributes to the lower slopes for stream water and groundwater. Similar slopes for stream water and groundwater further imply a high groundwater contribution to stream water (Ji et al., 2017). As expected, the slope (4.75) for the entire watershed (site BZA) falls within the range of slopes (4.13–6.52) for the five tributaries (Fig. 4b).

Stable isotopic signals for precipitation showed variations among the four seasons (Fig. 3b), with the highest $\delta^{18}O$ values observed in spring and lowest in summer. We did not observe a significant positive relationship between temperature and $\delta^{18}O$ values for precipitation (Dansgaard, 1964), which may result from other factors, such as precipitation amounts (negative relationship with $\delta^{18}O$ values) and different moisture sources (Song et al., 2017). The subtropical monsoon climate has a large amount of precipitation during the high temperature period (Fig. 2), which could mask the expected relationship. In addition, moisture sources for the study region vary seasonally, with winter moisture originating primarily from the north and west of China and from the South China Sea. In contrast, summer rainfall originates mostly from the Indian Ocean (Wang and Chen, 2012). When comparing seasonal variation in streamflow, $\delta^{18}O$ values (M_v) for the Yongan watershed were higher in spring (−6.11‰) and winter (−6.78‰) than in autumn (−7.20‰) and summer (−7.30‰), a similar seasonal pattern to that of precipitation (Fig. 3b). However, there were no significant ($p > 0.05$) correlations observed between $\delta^{18}O$ values and catchment characteristics (e.g., catchment area, elevation, topographic gradient and land-use proportions). This may result from the low number of catchments as well as interactions among multiple, complex hydrological processes within a given watershed.

The $\delta^{18}O$ and δ^2H values of stream water were less variable than that of precipitation as indicated by their lower standard deviations (Table 2). Additionally, precipitation showed a higher seasonal variation (amplitude: 1.81) than streamflow (amplitude: 0.25–0.64, Table 3). These findings further suggest that a substantial portion of stream water originates from older groundwater and subsurface water sources that consist of a temporal mixture of water inputs (Song et al., 2017). Across the six catchments, HG, BZA and ZK (amplitude: 0.53–0.64) had higher seasonal variation than GL, XZ and SJY (amplitude: 0.25–0.47) (Fig. 3b, Table 3). These differences in seasonal isotopic signals suggest contrasting hydrologic processes among the catchments.

3.2. Young water fraction and mean transit time dynamics

Estimated young water fractions (F_{yw}) for the six catchments in Yongan watershed ranged from 14 to 35% (Table 3), with the highest

Table 2
Summary of δ^2H (‰), $\delta^{18}O$ (‰), lc-excess (‰) and relationship between ^2H and ^{18}O in the Yongan watershed.

Sample	Site	Average δ^2H (‰)	Average $\delta^{18}O$ (‰)	Lc-excess (‰)	Slope (S) and intercept (I) for relationship between ^2H and ^{18}O
Precipitation	Yongan watershed[a]	−33.9 ± 24.1	−6.4 ± 2.9	–	S = 7.58, I = 14.66, n = 43, R^2 = 0.91**
Stream water	XZ[a]	−41.7 ± 4.9	−6.9 ± 0.7	−4.28	S = 5.61, I = −3.15, n = 44, R^2 = 0.59**
	HG[a]	−44.3 ± 6.2	−7.3 ± 1.1	−3.60	S = 4.66, I = −10.26, n = 47, R^2 = 0.68**
	SJY[a]	−38.0 ± 5.0	−6.2 ± 0.7	−5.85	S = 6.52, I = 2.24, n = 41, R^2 = 0.75**
	ZK[a]	−45.0 ± 6.6	−7.5 ± 1.1	−3.17	S = 4.97, I = −7.99, n = 38, R^2 = 0.64**
	GL[a]	−45.0 ± 4.9	−7.4 ± 0.9	−3.89	S = 4.13, I = −14.62, n = 47, R^2 = 0.53**
	BZA[a]	−42.8 ± 6.1	−6.9 ± 1.1	−5.39	S = 4.75, I = −10.16, n = 47, R^2 = 0.70**
Groundwater	ZK	−43.9 ± 6.1	−7.3 ± 1.1	−2.96	S = 4.59, I = −10.28, n = 42, R^2 = 0.73**
	BZA	−44.7 ± 3.3	−7.2 ± 0.9	−4.41	S = 2.38, I = −27.46, n = 47, R^2 = 0.42**

Superscript "a" represents volume-weighted mean. Values after " ± " are standard deviation. Lc-excess is abbreviation for line-conditioned excess. ** $p < 0.001$.

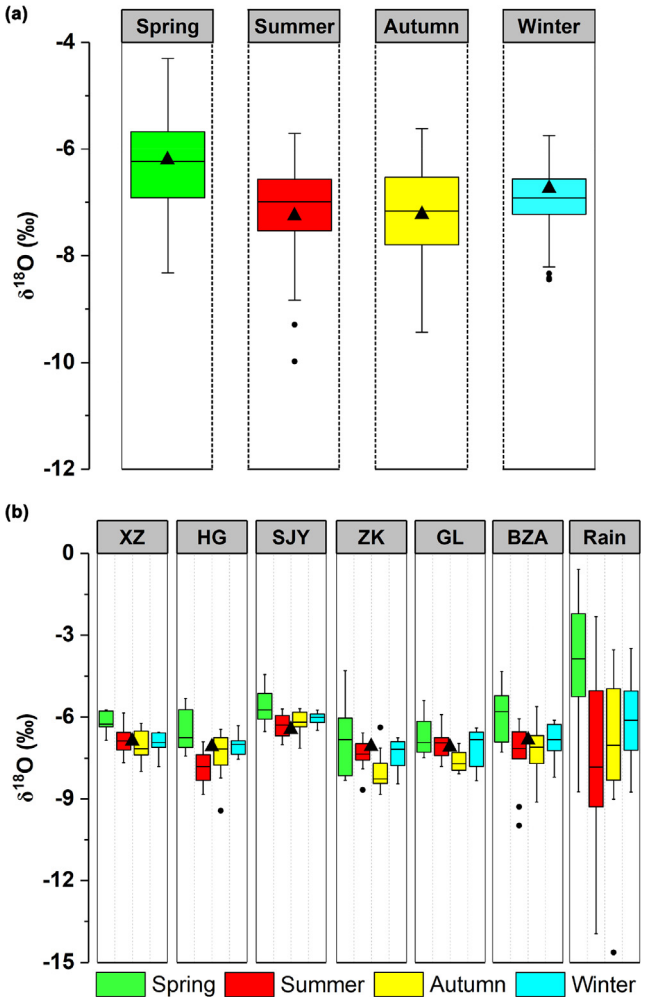

Fig. 3. Box plots for $\delta^{18}O$ in different seasons (a) in the Yongan River and several other rivers in China; and (b) across different water sampling sites and rainfall samples. Triangles represent the volume-weighted mean values (M_v). Square represents the M_v for the Yongan River. Box plots illustrate the 25th, 50th and 75th percentiles; whiskers indicate the 2.5th and 97.5th percentiles; points represent data outliers; and stars in panel (a) represent the minimum and maximum.

F_{yw} observed in ZK (35%) dominated by forest cover. In contrast, the lowest F_{yw} was observed in SJY (14%), which had the highest agricultural land use (Table 3). Estimated F_{yw} contributions suggest that the majority (on average 65–86%) of total streamflow may originate from slow subsurface lateral flow and groundwater. These results are consistent with the similar δ^2H and $\delta^{18}O$ values observed between stream water and groundwater (Table 2), as well as the similar slopes for the δ^2H vs $\delta^{18}O$ regression lines for stream water and groundwater (Fig. 4). The estimated slow flow proportion (67%) was also similar to the estimated average baseflow contribution of 84% determined by the Regional Nutrient Management (RuNuMa) model for the Yongan watershed (Hu et al., 2018). Overall, subsurface flow (e.g., relatively slow subsurface and groundwater flows) with a relatively older age is the major source of streamflow in the Yongan watershed. There were no significant correlations between F_{yw} and catchment area or different land-use characteristics, except for the fraction of non-utilized areas. The non-utilized lands include wild grasslands, barren lands with poor vegetation cover and water areas, which may facilitate greater surface runoff that contributes to the F_{yw} (Molina et al., 2012). The complex interplay between catchment characteristics might result in the insignificant relationships between F_{yw} and individual catchment characteristics (Lutz et al., 2018). In addition, uncertainties in the estimated F_{yw} values may contribute to the insignificant relationships, especially in those catchments with higher uncertainty ranges (e.g., ZK and BZA, Table 3).

Cumulative transit time distributions (TTD) showed the highest percentages of precipitation input travelling to the BZA and ZK outlets within 90 days, while that in SJY was the lowest (Fig. 5). These results are consistent with the F_{yw} rankings calculated from the seasonal $\delta^{18}O$ variations (Table 3). After transport of fast flow waters (i.e., short transit time water), the remaining water was transported more slowly through the catchments resulting in relatively long tails to the distributions. The TTD showed contrasting shapes among catchments (Fig. 5), which suggest hydrologic heterogeneities resulting from a complex interplay between catchment characteristics. For example, the distribution shape in HG catchment showed ~20% of the precipitation input travelled to the outlet within days, a likely consequence of high impervious surface area and storm drain efficiency (Yang and Toor, 2016).

By combining F_{yw} estimates with the TPLR approach, MTTs were determined to vary from 3.2 (catchment ZK) to 6.3 (catchment SJY) years across the six catchments (Table 3). These estimates are consistent with finding of high contributions from slow flows (65–86%) to streamflow as determined from F_{yw} analysis. Across the six catchments,

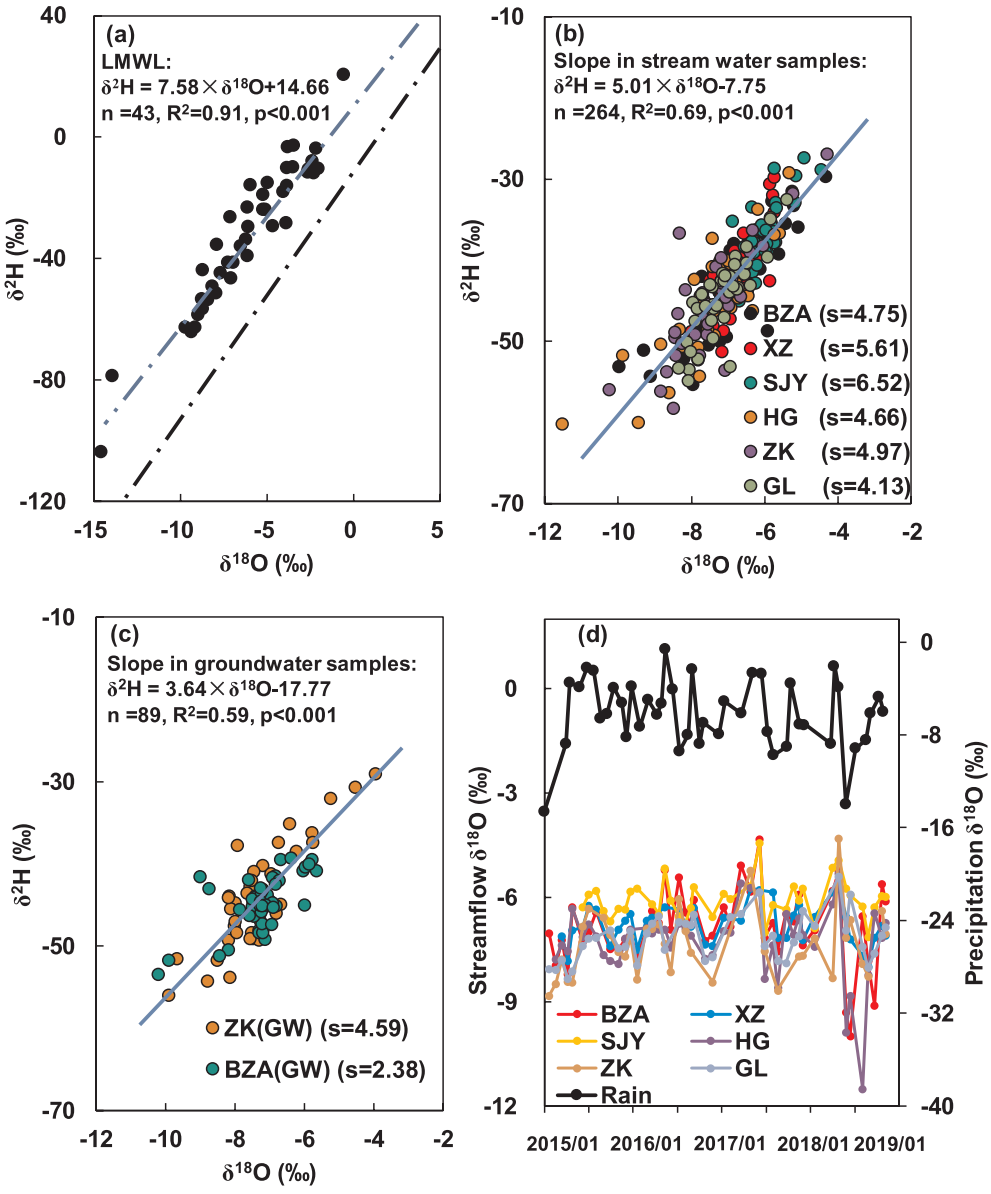

Fig. 4. Relationships between δ^2H and $\delta^{18}O$ for (a) precipitation, (b) stream water and (c) groundwater in Yongan watershed. Blue line represents the Local Meteoric Water Line (LMWL) in (a); Blue lines represent regression lines for surface water and groundwater samples in (b) and (c); black dot-dash line represents the Global Meteoric Water Line (GMWL), expressed as $^2H = 8 \times \delta^{18}O + 10‰$ ("s" in parenthesis represents slope of LMWL in different catchments). Temporal variations of $\delta^{18}O$ values in precipitation and stream water are presented in (d).

catchment area showed no significant relationship to estimated MTTs, suggesting the transit time was not strongly dependent on catchment scale, but more on topographic characteristics (McGuire et al., 2005). Although correlation analyses indicated no significant relationship between elevation and MTTs ($R^2 = 0.45$, $p = 0.146$, $n = 6$) across the six catchments, the relationship became significant ($R^2 = 0.88$, $p = 0.018$, $n = 5$) when catchment HG was removed. Similarly, the relationship between MTTs and topographic gradient became

Table 3
Estimated amplitude, young water fraction (F_{yw}) and mean transit time (MTT) in the Yongan watershed.

Catchment	Amplitude (‰)	Amplitude (95% C.L)	F_{yw}^a	F_{yw}^a (95% C.L)	F_{yw}^b	F_{yw}^b (95% C.L)	NSE	MTT (years)	MTT (95% C.L)
Precipitation	1.81	0.85–2.92	–	–	–	–	–	–	–
XZ	0.47	0.30–0.66	0.26	0.12–0.37	0.21	0.11–0.40	0.63	5.74	4.52–6.31
HG	0.53	0.28–0.81	0.29	0.11–0.47	0.28	0.15–0.54	0.59	5.11	4.91–5.93
SJY	0.25	0.10–0.51	0.14	0.04–0.26	0.15	0.04–0.32	0.56	6.33	6.02–6.35
ZK	0.64	0.30–1.01	0.35	0.17–0.84	0.34	0.20–0.65	0.47	3.19	2.35–3.72
GL	0.33	0.20–0.66	0.18	0.05–0.46	0.20	0.09–0.40	0.46	4.75	4.62–5.93
Entire watershed (BZA)	0.60	0.28–0.85	0.33	0.13–0.59	0.27	0.15–0.52	0.52	4.53	4.01–5.45

95% C.L represents the 95% confidence interval. NSE is the Nash-Sutcliffe efficiency comparing the modeled and measured stream water isotope concentrations. Superscript "a" represents the F_{yw} estimate based on $\delta^{18}O$ values; superscript "n" represents the F_{yw} estimated based on δ^2H values.

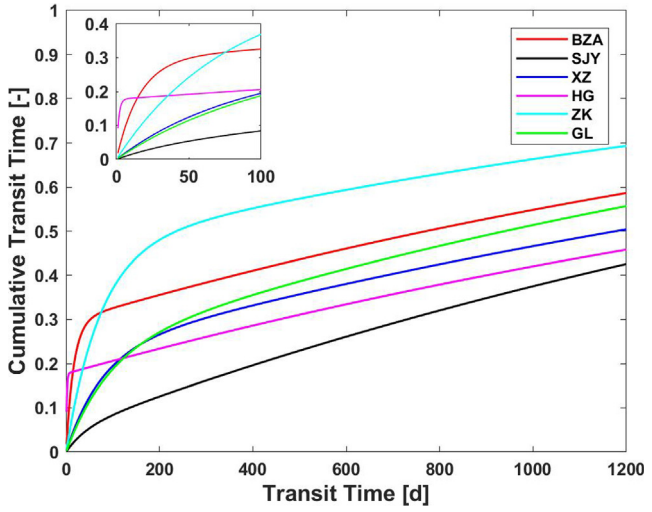

Fig. 5. Cumulated transit time distributions based on precipitation and stream water isotope data using the convolution integral. Inset shows zoomed 0–100 day transit times.

significant when the HG catchment was removed (R^2 = 0.82, p = 0.036, n = 5). The negative relationship between MTTs and topographic gradient is explainable by the gravitational influence on hydraulic gradients that are the driving force for water flows (e.g., overland flow and sub-surface flow, McGuire et al., 2005; Tetzlaff et al., 2009). However, no significant relationship between MTTs and topographic wetness index (TWI) was observed (R^2 = 0.24, p = 0.33, n = 6), even if the HG catchment was removed (R^2 = 0.68, p = 0.084, n = 5). Additionally, no significant correlations (p > 0.05) were observed between MTTs and land-use fractions or drainage density. Therefore, only a few topographic characteristics (e.g., elevation and topographic gradient) appear to have a strong influence on the spatial distribution of MTTs in the Yongan watershed. However, it must be noted that the low number of catchments coupled with the sometimes-large uncertainties associated with the MTT estimates limit the power of correlation analysis to identify possible associations.

The estimates of F_{yw} and MTT were not significantly correlated (R^2 = 0.56, p = 0.088, n = 6). This may be due to the uncertainties in F_{yw} and MTT, as well as the low number (n = 6) of catchments available for the correlation analysis. Contrasting subsurface flow components among the six catchments may also contribute to differences between the F_{yw} and MTT metrics. For the Yongan watershed, our results indicated that subsurface flows (i.e., relatively slow subsurface flow and groundwater) were the major contributor to streamflow (Table 3, Hu et al., 2018), resulting in relatively long MTTs. Also, the high sensitivity of MTT to slow flow (τ_s) highlights the important role of slow flowpaths on MTT estimates (Fig. 6a). As indicated by previous studies, subsurface flows vary considerably due to differences in soil depth, rock type/conductivity and groundwater aquifers resulting in a considerable range of water ages (Szabo et al., 1996; Manning et al., 2012). Due to these differences in topographic and geologic attributes, catchments with smaller F_{yw} may also have greater contributions from deeper flowpaths having longer residence times. Overall, combining the analysis of F_{yw} and MTTs provides a more robust understanding of watershed-scale hydrological processes.

In this study, no significant difference was noted between F_{yw} estimates based on δ^2H versus $\delta^{18}O$ (Table 3), suggesting that both δ^2H and $\delta^{18}O$ values equally capture the seasonal variations in stable isotope composition. In contrast, MTT estimates based on δ^2H resulted in a lower NSE than for $\delta^{18}O$-based estimates. This may result from the strong evapotranspiration (Fig. 2b, Table 2) in our subtropical watershed leading to preferential fractionation of δ^2H in the water flows (Bansah and Ali, 2019). In general, it is considered more appropriate to use $\delta^{18}O$ values in systems with high evapotranspiration (Bansah and Ali, 2019).

3.3. Uncertainty and sensitivity analyses

As a first attempt to improve MTT estimates by including F_{yw} constraints in a subtropical watershed in eastern China, we document unavoidable uncertainty associated with four years of monthly measurements for $\delta^{18}O$ and δ^2H. The 95% confidence intervals for F_{yw} estimates using 4 years of stable isotope data varied across catchments, with the largest uncertainty observed in ZK and smallest in SJY (Table 3). The sources of uncertainty may be associated with the sampling strategies across space and time. The monthly sampling frequency for both precipitation and streamflow is prone to missing seasonal extremes in the stable isotope signals, which generally result in underestimation of seasonal amplitudes (Lutz et al., 2018). Additionally, isotope records for a single precipitation sampling site may not be representative of the entire watershed. Uncertainty appeared related to the distance of the streamflow sampling sites from the precipitation collection site, with larger uncertainty in catchments (e.g., GL and ZK) located farther away from the precipitation sampling site (Fig. 1). According to the negative correlation between elevation and $\delta^{18}O$ values in precipitation (Bowen and Wilkinson, 2002), the precipitation isotopic composition at lower elevations (Table 1, Fig. 1) would be expected to result in higher amplitudes for the precipitation and thus smaller F_{yw} values in these catchments. Due to differences of elevation (Table 1), the single precipitation sampling site in XZ may lead to an overestimation of F_{yw} in HG and an underestimation of F_{yw} in ZK. Therefore, we assumed a 20% increase of precipitation amplitudes for HG and a 20% decrease for ZK

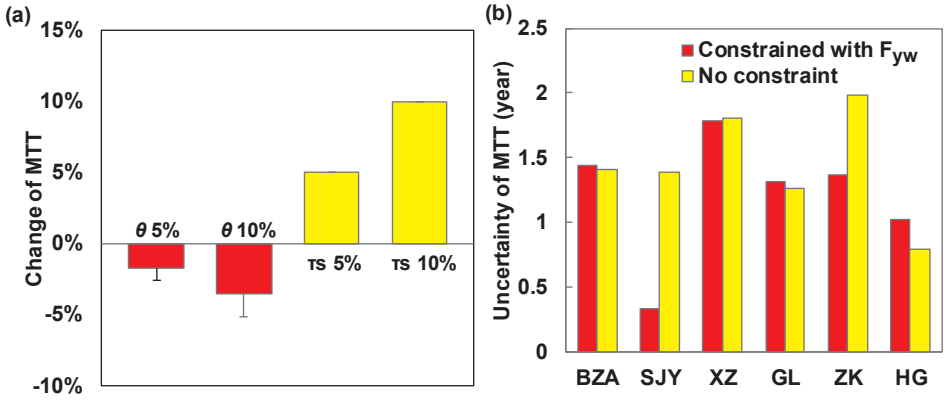

Fig. 6. Histograms of (a) sensitivity analysis results for MTT and (b) differences of estimated MTTs between optimization methods with and without F_{yw} constraints. "5/10%" represents 5 or 10% change in θ (i.e., F_{yw}) and τ_s in sensitivity analysis.

in the uncertainty analysis (Table 3). Additionally, the use of estimated discharge volumes for sub-catchments could introduce uncertainties in calculation of volume-weighted mean values for each sub-catchment.

Sensitivity analysis indicated differential MTT sensitivity to θ, τ_f and τ_s in the two-parallel linear reservoir model; results indicated that a 5% increase of θ, τ_f and τ_s produced a ~2% increase, 0% and ~5% decrease of MTT, respectively (Fig. 6a). Across the six catchments, the sensitivity of θ showed more variability than that of τ_s (Fig. 6a), with higher θ variability accompanied by larger F_{yw}. This result emphasizes the importance of constraining θ and τ_s values in determining MTTs. The estimated 95% confidence intervals for MTTs also varied across catchments, with the largest uncertainty observed in XZ and smallest in SJY (Table 3). When comparing the estimated MTTs between optimization methods with and without F_{yw} constraints, results indicated a decrease in the uncertainty of MTTs with F_{yw} constraints, especially in catchments SJY and ZK (Fig. 6b). MTT sensitivity to θ and the reduction of MTT uncertainty in some catchments suggest the potential benefits of combining F_{yw} constraints in estimating MTTs (Lutz et al., 2018).

Due to the spatial and temporal variability of estimated F_{yw} and MTTs, long-term sampling is necessary to more rigorously characterize hydrological processes at the watershed scale. Previous studies suggested that the robustness of F_{yw} estimates is related to sampling frequency, highlighting that a higher sampling frequency may be necessary to effectively capture seasonal and storm-event streamflow dynamics (Stockinger et al., 2016). A more rigorous sampling regime during storm events (such as collecting water samples before, during and after a storm event) may be necessary to capture uncertainties associated with short-term storm events (Swarowsky et al., 2012). The lack of significant correlations between F_{yw} and many hydrologically relevant landscape and hydro-climate characteristics was limited by the number catchments ($n = 6$) and the relatively narrow range in characteristics among catchments. Therefore, increasing the numbers of catchments to optimize differences in land use/land cover, geology, soils and topographic characteristics would provide a more robust dataset for exploring potential influencing factors and their interactions.

Considering the limited number of sampling sites used to collect precipitation and groundwater in this study (one precipitation collection site and two groundwater monitoring wells, Fig. 1), it is highly warranted to increase the number of sampling sites, such as paired precipitation, groundwater and streamflow samples in each catchment. Continuous streamflow measurements for each sub-catchment would further constrain the uncertainty associated with analyses requiring stream discharge values. With a higher sampling frequency, a quantitative prediction of evaporation based on the revised Craig–Gordon model (Skrzypek et al., 2015) is possible to assess the role of evapotranspiration in $\delta^{18}O$ and $\delta^{2}H$ dynamics and F_{yw} and MTT uncertainties. Additional studies incorporating other tracers (e.g., chlorofluorocarbons, tritium, etc.) are planned to further explore the spatial variation of groundwater age and its relationship to F_{yw} and MTTs (Busenberg and Plummer, 1992; Stewart et al., 2010). This study highlights that field sampling modifications and improvement in future studies will better capture the spatial and temporal dynamics associated with $\delta^{18}O$ and $\delta^{2}H$ dynamics at the watershed scale.

3.4. Implications for water resource management

The combination of F_{yw}, TTDs and MTTs provide important information on water cycling in hydrological systems. The low F_{yw} and long MTTs (Table 3) identified in this study highlight the critical need to appropriately exploit and protect groundwater resources for sustainable water management in the Yongan watershed. For example, in agricultural catchments (e.g., SJY and GL) using groundwater for irrigation, the high groundwater contributions to streamflow highlight the importance of developing appropriate water management practices to avoid groundwater over-exploitation. High contributions of relatively slow subsurface flows and groundwater to streamflow provide economically and ecologically important streamflow during the dry season and especially in dry years. Therefore, monitoring to avoid groundwater over-exploitation should be implemented to promote sustainable water resource management and utilization. Additionally, the Yongan watershed frequently suffers flooding during the typhoon season and extreme weather events are expected to increase based on climate change projections. Our results inform watershed modeling studies addressing potential mitigation strategies to attenuate extreme weather events, such as dam/reservoir construction to provide flood/drought water storage capacity.

In terms of water quality, the different travel time distributions among catchments emphasize the need for different management strategies to address pollution control. For catchments with high F_{yw} (e.g., ZK and HG), the rapid transport of precipitation to streams requires beneficial management practices (BMPs) that target the quick flushing of pollutants from residential areas to surface waters, such as enhanced infiltration (e.g., porous pavement, infiltration trenches and swales) and interception methods (e.g., wetlands, buffer strips). For watersheds with large contributions of subsurface flow and groundwater, relatively long MTTs imply a considerable lag effect in the response of water quality to changes in pollution inputs and BMPs at the watershed scale. For a watershed with a MTT of 4.5 years, it would take more than 4.5 years for pollutants to be delivered from a source area to the watershed outlet. Therefore, environmental managers may ignore negative impacts from human activities (e.g., excessive fertilizer and manure applications) on stream water quality, since water quality impairment might only be detected several years following pollution release by human activities. For example, our previous water quality modeling results suggest a ~10 year lag-time for nitrogen inputs to be leached/transported from the Yongan watershed (Chen et al., 2014a; Hu et al, 2018). Once groundwater and river water pollution are detected, the slow delivery of groundwater pollutants would result in persistent water quality impairment even after implementation of relevant pollution control measures (e.g., reduction in pollutant sources; Meals et al., 2010; Hamilton, 2012). Such legacy effects have been widely observed in many watersheds worldwide (Meals et al., 2010). Given the nutrient pollution issues observed in the Yongan watershed (Chen et al., 2014b; Hu et al., 2019), we highlight the need for water pollution control strategies that also focus on groundwater protection and restoration (Thiruvenkatachari et al., 2008; Siegrist et al., 2011).

4. Conclusions

Based on a four-year record for stable isotopes of oxygen and hydrogen for precipitation, stream water and groundwater, this study quantified the young water fraction (F_{yw}) and used the F_{yw} to constrain/optimize estimates of mean transit time (MTT) in a typical subtropical watershed of eastern China. Isotope signals across precipitation, groundwater and stream water demonstrated the impacts of evapotranspiration and transient groundwater storage on streamflow generation, implying delayed transport of water from precipitation to streamflow. Estimated F_{yw} ranged from 14 to 35%, while MTTs ranged from 3.2 to 6.3 years across the six catchments. The cumulative transit time showed varying distributions, suggesting appreciable heterogeneity and a complex interplay between catchment characteristics. MTTs were significantly correlated with elevation and topographic gradient in catchments with low human impacts. The use of F_{yw} to constrain MTT estimates resulted in lower uncertainty in some catchments. The relatively low F_{yw} and long MTTs suggest that groundwater plays a key component in watershed streamflow generation and introduces a considerable lag time to water quantity and quality responses to land management measures and climate change. A higher sampling frequency (especially during storm events), addition of more diverse sampling sites and a longer sampling duration are warranted to reduce uncertainties in the estimated F_{yw} and MTT values. This study fills a "gap" in $\delta^{18}O$ and $\delta^{2}H$ maps for subtropical rivers in eastern

China. Further, the results improve insights for elucidating hydrologic process identification and hydrograph separation, thereby enhancing our understanding of watershed-scale hydrological processes to guide water resource management.

CRediT authorship contribution statement

Minpeng Hu: Data curation, Methodology, Software, Validation. **Yufu Zhang:** Methodology, Investigation, Data curation. **Kaibin Wu:** Methodology, Software, Validation. **Hong Shen:** Investigation, Data curation. **Mengya Yao:** Investigation, Data curation. **Randy A. Dahlgren:** Conceptualization, Writing - review & editing. **Dingjiang Chen:** Conceptualization, Methodology, Validation, Formal analysis, Investigation, Writing - review & editing, Supervision.

Declaration of Competing Interest

The authors declare that they have no known competing financial interests or personal relationships that could have appeared to influence the work reported in this paper.

Acknowledgements

We thank local government departments for providing relevant data for this investigation. This work was supported by the Zhejiang Provincial Natural Science Foundation of China (LR19D010002), National Natural Science Foundation of China (41877465 and 51679210), and National Key Research and Development Program of China (2017YFD0800101).

Appendix A. Supplementary data

Supplementary data to this article can be found online at https://doi.org/10.1016/j.jhydrol.2020.125363.

References

Babkin, V.I., 2009. Evaporation from the surface of the globe. In: In: Shiklomanov, I.A. (Ed.), Hydrological Cycle, vol. 2 EOLSS, Paris.
Bansah, S., Ali, G., 2019. Streamwater ages in nested, seasonally cold Canadian watersheds. Hydrol. Process. 33, 495–511.
Beven, K., Kirkby, M.J., 1979. A physically based, variable contributing area model of basin hydrology. Hydrol. Sci.-Bull. 24, 43–69.
Biswas, A.K., 2004. Integrated water resources management: a reassessment. A water forum contribution. Water Int. 29 (2), 248–256.
Bowen, G.J., Wilkinson, B., 2002. Spatial distribution of $\delta^{18}O$ in meteoric precipitation. Geology 30 (4), 315–318.
Brand, W.A., Coplen, T.B., Vogl, J., Rosner, M., Prohaska, T., 2014. Assessment of international reference materials for isotope-ratio analysis (IUPAC Technical Report). Pure Appl. Chem. 86, 425–467.
Busenberg, E., Plummer, L.N., 1992. Use of chlorofluorocarbons (CCl_3F and CCl_2F_2) as hydrologic tracers and age-dating tools: the alluvium and terrace system of central Oklahoma. Water Resour. Res. 28, 2257–2283.
Buttle, J.M., 1994. Isotope hydrograph separations and rapid delivery of pre-event water from drainage basins. Prog. Phys. Geogr. 18 (1), 16–41.
Chen, D.J., Hu, M.P., Dahlgren, R.A., 2014a. A dynamic watershed model for determining the effects of transient storage on nitrogen export to rivers. Water Resour. Res. 50 (10), 7714–7730.
Chen, D.J., Huang, H., Hu, M.P., Dahlgren, R.A., 2014b. Influence of lag effect, soil release, and climate change on watershed anthropogenic nitrogen inputs and riverine export dynamics. Environ. Sci. Technol. 48, 5683–5690.
Clow, D.W., Mast, M.A., Sickman, J.O., 2018. Linking transit times to catchment sensitivity to atmospheric deposition of acidity and nitrogen in mountains of the western United States. Hydrol. Process. 32 (16), 2456–2470.
Craig, H., 1961. Isotopic variations in meteoric waters. Science 133, 1702–1703.
Dansgaard, W., 1964. Stable isotopes in precipitation. Tellus 16 (4), 436–468.
Davis Todd, C.E., Goss, A.M., Tripathy, D., Harbor, J.M., 2007. The effects of landscape transformation in a changing climate on local water resources. Phys. Geogr. 28, 21–36.
Gonfiantini, R., 1986. Environmental isotopes in lake studies. Handbook of Environmental Isotope Geochemistry; The Terrestrial Environment, pp. 113-168.
Hale, V.C., McDonnell, J.J., 2016. Effect of bedrock permeability on stream base flow mean transit time scaling relations: 1. A multiscale catchment intercomparison. Water Resour. Res. 52 (2), 1358–1374.
Hamilton, S.K., 2012. Biogeochemical time lags may delay responses of streams to ecological restoration. Freshw. Biol. 57, 43–57.
Hangen, E., Lindenlaub, M., Leibundgut, C., Von Wilpert, K., 2001. Investigating mechanisms of stormflow generation by natural tracers and hydrometric data: a small catchment study in the Black Forest, Germany. Hydrol. Processes 15 (2), 183–199.
Hrachowitz, M., Soulsby, C., Tetzlaff, D., Dawson, J.J.C., Dunn, S.M., Malcolm, I.A., 2009. Using long-term data sets to understand transit times in contrasting headwater catchments. J. Hydrol. 367 (3), 237–248.
Hrachowitz, M., Soulsby, C., Tetzlaff, D., Speed, M., 2010. Catchment transit times and landscape controls—does scale matter? Hydrol. Processes: Int. J. 24 (1), 117–125.
Hu, C.H., Froehlich, K., Zhou, P., Lou, Q., Zeng, S.M., Zhou, W.B., 2013. Seasonal variation of oxygen-18 in precipitation and surface water of the Poyang Lake Basin, China. Isot. Environ. Health Stud. 49, 188–196.
Hu, M.P., Liu, Y.M., Wang, J.H., Dahlgren, R.A., Chen, D.J., 2018. A modification of the Regional Nutrient Management model (ReNuMa) to identify long-term changes in riverine nitrogen sources. J. Hydrol. 561, 31–42.
Hu, M.P., Liu, Y.M., Zhang, Y.F., Dahlgren, R.A., Chen, D.J., 2019. Coupling stable isotopes and water chemistry to assess the role of hydrological and biogeochemical processes on riverine nitrogen sources. Water Res. 150, 418–430.
Jakeman, A.J., Hornberger, G.M., 1993. How much complexity is warranted in a rainfall-runoff model? Water Resour. Res. 29 (8), 2637–2649.
Jasechko, S., Kirchner, J.W., Welker, J.M., McDonnell, J.J., 2016. Substantial proportion of global streamflow less than three months old. Nat. Geosci. 9, 126–129.
Jasechko, S., Wassenaar, L.I., Mayer, B., 2017. Isotopic evidence for widespread cold-season-biased groundwater recharge and young streamflow across central Canada. Hydrol. Process. 31 (12), 2196–2209.
Ji, X.L., Xie, R.T., Hao, Y., Lu, J., 2017. Quantitative identification of nitrate pollution sources and uncertainty analysis based on dual isotope approach in an agricultural watershed. Environ. Pollut. 229, 586–594.
Kennedy, J., Eberhart, R., 1995. Particle swarm optimization. In: Proceedings of the IEEE International Conference on Neural Networks, pp. 1942–1948.
Kirchner, J.W., 2016. Aggregation in environmental systems–part 1: seasonal tracer cycles quantify young water fractions, but not mean transit times, in spatially heterogeneous catchments. Hydrol. Earth Syst. Sci. 20, 279–297.
Klaus, J., McDonnell, J.J., 2013. Hydrograph separation using stable isotopes: Review and evaluation. J. Hydrol. 505, 47–64.
Kværner, J., Kløve, B., 2006. Tracing sources of summer streamflow in boreal headwaters using isotopic signatures and water geochemical components. J. Hydrol. 331 (1–2), 186–204.
Landwehr, J.M., Coplen, T.B., 2006. Line-conditioned excess: a new method for characterizing stable hydrogen and oxygen isotope ratios in hydrologic systems. In: International Conference on Isotopes in Environmental Studies. IAEA, Vienna, pp. 132–135.
Li, S.L., Yue, F.J., Liu, C.Q., Ding, H., Zhao, Z.Q., Li, X., 2015. The O and H isotope characteristics of water from major rivers in China. Chin. J. Geochem. 34, 28–37.
Lutz, S.R., Krieg, R., Müller, C., Zink, M., Knöller, K., Samaniego, L., Merz, R., 2018. Spatial patterns of water age: using young water fractions to improve the characterization of transit times in contrasting catchments. Water Resour. Res. 54, 4767–4784.
Manning, A.H., Clark, J.F., Diaz, S.H., Rademacher, L.K., Earman, S., Plummer, L.N., 2012. Evolution of groundwater age in a mountain watershed over a period of thirteen years. J. Hydrol. 460, 13–28.
McGuire, K.J., McDonnell, J.J., 2006. A review and evaluation of catchment transit time modeling. J. Hydrol. 330, 543–563.
McGuire, K.J., McDonnell, J.J., 2010. Hydrological connectivity of hillslopes and streams: characteristic time scales and nonlinearities. Water Resour. Res. 46 (10), W10543.
McGuire, K.J., McDonnell, J.J., Weiler, M., Kendall, C., McGlynn, B.L., Welker, J.M., Seibert, J., 2005. The role of topography on catchment-scale water residence time. Water Resour. Res. 41, W05002.
Meals, D.W., Dressing, S.A., Davenport, T.E., 2010. Lag time in water quality response to best management practices: a review. J. Environ. Qual. 39, 85–96.
Mokhtar, A., He, H.M., Zhao, H.F., Keo, S., Bai, C.Y., Zhang, C.J., Ma, Y., Ibrahim, A., Li, F.J., He, W.M., Abdo, A.I., Zhou, J., 2020. Risks to water resources and development of a management strategy in the river basins of the Hengduan Mountains, Southwest China. Environ. Sci. Water Res. Technol. 6, 656–678.
Molina, A., Vanacker, V., Balthazar, V., Mora, D., Govers, G., 2012. Complex land cover change, water and sediment yield in a degraded Andean environment. J. Hydrol. 472, 25–35.
Nash, J.E., Sutcliffe, J.V., 1970. River flow forecasting through conceptual models: part I – a discussion of principles. J. Hydrol. 10 (3), 282–290.
Pinder, G.F., Jones, J.F., 1969. Determination of the ground-water component of peak discharge from the chemistry of total runoff. Water Resour. Res. 5 (2), 438–445.
Sánchez-Murillo, R., Brooks, E.S., Elliot, W.J., Boll, J., 2015. Isotope hydrology and base flow geochemistry in natural and human-altered watersheds in the Inland Pacific Northwest, USA. Isot. Environ. Health Stud. 51, 231–254.
Seeger, S., Weiler, M., 2014. Reevaluation of transit time distributions, mean transit times and their relation to catchment topography. Hydrol. Earth Syst. Sci. 18 (12), 4751–4771.
Siegrist, R.L., Crimi, M., Simpkin, T.J., 2011. In Situ Chemical Oxidation for Groundwater Remediation. Springer Science & Business Media, New York, NY.
Skrzypek, G., Mydłowski, A., Dogramaci, S., Hedley, P., Gibson, J.J., Grierson, P.F., 2015. Estimation of evaporative loss based on the stable isotope composition of water using *Hydrocalculator*. J. Hydrol. 523, 781–789.
Song, C., Wang, G., Liu, G., Mao, T., Sun, X., Chen, X., 2017. Stable isotope variations of precipitation and streamflow reveal the young water fraction of a permafrost watershed. Hydrol. Process. 31, 935–947.

Sörensen, R., Zinko, U., Seibert, J., 2006. On the calculation of the topographic wetness index: evaluation of different methods based on field observations. Hydrol. Earth Syst. Sci. Discuss. 10 (1), 101–112.
Stewart, M.K., Morgenstern, U., McDonnell, J.J., 2010. Truncation of stream residence time: How the use of stable isotopes has skewed our concept of streamwater age and origin. Hydrol. Process. 24, 1646–1659.
Stockinger, M.P., Bogena, H.R., Lücke, A., Diekkrüger, B., Cornelissen, T., Vereecken, H., 2016. Tracer sampling frequency influences estimates of young water fraction and streamwater transit time distribution. J. Hydrol. 541, 952–964.
Swarowsky, A., Dahlgren, R.A., O'Geen, A.T., 2012. Linking subsurface lateral flowpath activity with streamflow characteristics in a semiarid headwater catchment. Soil Sci. Soc. Am. J. 76 (2), 532–547.
Szabo, Z., Rice, D.E., Plummer, L.N., Busenberg, E., Drenkard, S., Schlosser, P., 1996. Age dating of shallow groundwater with chlorofluorocarbons, tritium/helium: 3, and flow path analysis, Southern New Jersey Coastal Plain. Water Resour. Res. 32 (4), 1023–1038.
Tetzlaff, D., Seibert, J., McGuire, K.J., Laudon, H., Burns, D.A., Dunn, S.M., Soulsby, C., 2009. How does landscape structure influence catchment transit time across different geomorphic provinces? Hydrol. Process.: Int. J. 23 (6), 945–953.
Thiruvenkatachari, R., Vigneswaran, S., Naidu, R., 2008. Permeable reactive barrier for groundwater remediation. J. Ind. Eng. Chem. 14 (2), 145–156.
Timbe, E., Windhorst, D., Crespo, P., Frede, H.G., Feyen, J., Breuer, L., 2014. Understanding uncertainties when inferring mean transit times of water trough tracer-based lumped-parameter models in Andean tropical montane cloud forest catchments. Hydrol. Earth Syst. Sci. 18 (4), 1503–1523.
von Freyberg, J., Allen, S.T., Seeger, S., Weiler, M., Kirchner, J.W., 2017. Sensitivity of young water fractions to hydro-climatic forcing and landscape properties across 22 Swiss catchments. Hydrol. Earth Syst. Sci. 22, 3841–3861.
Vrugt, J.A., 2016. Markov chain Monte Carlo simulation using the DREAM software package: theory, concepts, and MATLAB implementation. Environ. Modell. Software 75, 273–316.
Wang, H.J., Chen, H.P., 2012. Climate control for southeastern China moisture and precipitation: Indian or East Asian monsoon? J. Geophys. Res.: Atmos. 117 (D12109). https://doi.org/10.1029/2012JD017734.
Wang, S.Q., Yuan, R.Q., Tang, C.Y., Song, X.F., Currell, M., Yang, Z.L., Sheng, Z.P., 2018. Combination of CFCs and stable isotopes to characterize the mechanism of groundwater–surface water interactions in a headwater basin of the North China Plain. Hydrol. Process. 32 (11), 1571–1587.
Weiler, M., McGlynn, B.L., McGuire, K.J., McDonnell, J.J., 2003. How does rainfall become runoff? A combined tracer and runoff transfer function approach. Water Resour. Res. 39 (11), 1315–1327.
Wilusz, D.C., Harman, C.J., Ball, W.P., 2017. Sensitivity of catchment transit times to rainfall variability under present and future climates. Water Resour. Res. 53 (12), 10231–10256.
Yang, Y.Y., Toor, G.S., 2016. $\delta^{15}N$ and $\delta^{18}O$ reveal the sources of nitrate-nitrogen in urban residential stormwater runoff. Environ. Sci. Technol. 50 (6), 2881–2889.